Electronic Supplementary Information (ESI)

for

Pillararene-functionalized rhodium nanoparticles for efficient catalytic reduction and photothermal sterilization

Qinglan Li, [a] Li Ji, [a] Beibei Jiang, [c] Xiangguang Li, [a] Zhaoji Lv, [a] Jinpo Xie, [a] Siping Chen, [a] Kailin Xu,[a]* Yingwei Yang,[b]* and Suqing Zhao [a]*

[a]Department of Pharmaceutical Engineering, School of Biomedical and Pharmaceutical Sciences, Guangdong University of Technology, Guangzhou 510006, P. R. China

[b]International Joint Research Laboratory of Nano-Micro Architecture Chemistry, College of Chemistry, Jilin University, 2699 Qianjin Street, Changchun 130012, P. R. China

[c]Analysis and Test Center, Guangdong University of Technology, Guangzhou 510006, P. R. China

*E-mail addresses: xukailin@gdut.edu.cn, ywyang@jlu.edu.cn, sqzhao@gdut.edu.cn

Materials

Carboxylated pillar[5]arene sodium salt (CPA) was prepared according to our previous report,[S1] $RhCl_3 \cdot 3H_2O$ was purchased from Beijing InnoChem Science & Technology Co., Ltd., $NaBH_4$ was obtained from Tianjin Fucheng Chemical Reagent Factory, nitrophenols from Shanghai Macklin Biochemical Co., Ltd, and methyl orange (MO) and congo red (CR) from Tianjin Damao Chemical Reagent Factory. All the reagents with analytically pure were directly used without further purification. *Staphylococcus aureus* (ATCC 6538, *S. aureus*) was purchased from the Guangdong Microbial Culture Collection Center (GDMCC, China).

Characterization

The morphology of Rh@CPA was observed on transmission electron microscopy (TEM, Talos F200S), and the crystallographic texture was verified by an X-ray diffractometer (XRD, Bruker D8 ADVANCE) equipped with Cu Kα radiation. X-ray photoelectron spectroscopy (XPS, Thermo Fisher Escalab 250Xi) was employed to identify the chemical valence of elements. The concentration of Rh@CPA was measured by inductively coupled plasma mass spectrometry (ICP-MS, Thermo Fisher ICAP RQ). UV–vis absorption spectra were collected on a PerkinElmer Lambda 950. Infrared spectroscopy (IR) analysis was carried out on a Thermo Fisher iS50R. 808 nm laser was obtained from Xi'an Herschel Laser technology company. Leica EM CPD300 and Hitachi SU8010 were used to prepare samples and capture the morphology of *S. aureus*, respectively.

Preparation of Rh@CPA NPs

$RhCl_3$ $3H_2O$ (6 mg/mL, 250 mL) was added into deionized water (5.0 mL) containing 0.2 times of CPA (12 mg/mL, 333 mL). Then $NaBH_4$ (2 mg/mL, 250 μL) was poured into the above solution, and the mixture changed dark immediately. After being stirred for 30 min at room temperature, the reaction mixture was purified by dialyzing with a cellulose ester membrane bag (molecular weight cutoff = 3000) for 5 days to remove the unreacted Rh ions and CPA. The obtained Rh@CPA NPs were characterized by TEM, XRD, XPS, IR spectroscopy, and UV-vis spectroscopy and stored at 4 °C for further use.

Catalytic reduction of nitrophenol isomers by using Rh@CPA NPs

Nitrophenol and deionized water were added to a standard quartz cuvette. When freshly

prepared $NaBH_4$ was added, the color of the mixture changed from light-yellow to yellow-green immediately as a consequence of the formation of nitrophenolate ion. Rh@CPA NPs were added, and the UV-vis absorption spectra were recorded in the range of 200-600 nm at various time intervals (2 min, 1.5 min, and 1.5 min for 4-nitrophenol, 3-nitrophenol, and 2-nitrophenol, respectively). The final volume of the reaction solution was 3.3 mL, and concentrations of 4-, 3-, and 2-nitrophenol were 0.1 mM, 0.6 mM, 0.2 mM. Detailed information is provided in Table S1.

Table S1. The detailed experimental parameters of the catalytic reductions for nitrophenols by using the Rh@CPA catalyst

Nitrophenols	Amount of nitrophenols (3.0 mM)	Amount of $NaBH_4$ (0.1 M)	Amount of catalyst (29 μg/mL)
4-nitrophenol	110 μL	300 μL	66 μL
3-nitrophenol	660 μL	300 μL	66 μL
2-nitrophenol	220 μL	300 μL	66 μL

Catalytic degradation of MO and CR by using Rh@CPA

MO or CR (3.0 mM, 110 mL) and deionized water (2.824 mL) were poured into a standard quartz cuvette. Then freshly $NaBH_4$ (0.1 M, 300 mL) and Rh@CPA (29.6 μg/mL, 66 μL) were added. The UV-vis absorption spectra were finally collected in the range of 300-650 nm at a time interval of 1.5 min.

Photothermal performance test of Rh@CPA

An aqueous suspension of Rh@CPA NPs (1 mL) was illuminated with an 808 nm laser at an output power density of 1 W/cm^2 for 7 min. The increase and decrease in temperature were recorded by a photothermal imager every 20 s and 60 s, respectively. The photothermal performance test was repeated 5 times to determine the photothermal stability of the sample. The photothermal conversion efficiency (η) of Rh@CPA was calculated according to the following equations.[S2,S3]

$$t = -\tau_s Ln\theta = -\tau_s Ln\frac{T_{sur}-T}{T_{sur}-T_{max}} \quad (a)$$

$$\tau_s = \frac{m_D C_D}{hS} \quad (b)$$

$$\eta = \frac{hS(T_{max}-T_{sur})-Q_{dis}}{I(1-10^{-A_{808}})} \quad (c)$$

τ_s represents the time constant of the sample, T_{sur} and T_{max} are the ambient and equilibrium maximum temperatures, respectively, and T is the temperature of the sample during the cooling process. S is the surface area of the container, h is the heat transfer coefficient, Q_{dis} represents the heat dissipation ascribed to absorption of the solvent and quartz sample cell, I is the laser power, and A808 is the absorbance of Rh@CPA at 808 nm.

Photothermal antibacterial

To achieve exponential growth, *S. aureus* was cultured in LB medium under 220 rpm shaking at 37 ºC for about 15 h, which was then diluted 10 000 times. Sequentially, 40 mL of diluted *S. aureus* solution was mixed with Rh@CPA solutions at different concentrations of 0, 6.25, 12.50, and 25.00 μg/mL and irradiated by an 808 nm laser with a power density of 1.0 W/cm^2 for 7 min. After being incubated in a shaker at 220 rpm and 37 ºC for 4 h, 50 μL of the above *S. aureus* solution was spread on the agar plate medium and cultured for another 15 h at 37 ºC to evaluate the photothermal antibacterial effect.

Biocompatibility assessment

In vitro cytotoxicity of Rh@CPA was evaluated by the CellTiter-Glo luminescence assay according to the ATP level for NCTC clone 929 (L929) cells. The L929 cells were cultured in Dulbecco's Modified Eagle Medium (DMEM) at 37 ºC and 5% CO_2, seeded onto 96-well plates at a density of 2.5 × 10^4/well and cultured in 96-well plates. When completely attached to the plates, the L929 cells were incubated in the DMEM with increasing Rh@CPA concentrations (1.56 to 25.00 μg/mL) for another 24 h. Then the cells were washed with PBS three times, replaced with the fresh medium containing 50 μL CellTiter-GLO substrate and 50 μL PBS, and incubated at room temperature for 4 min. Finally, the luminescence was recorded using BioTek FLx800 Fluorescence Microplate Reader.

To further evaluate the biocompatibility of Rh@CPA, Rh NPs solution (25 μg/mL, 100 μL) and saline were injected into female SD rats, respectively. After 48 h, the mice were sacrificed,

and their major tissues (heart, liver, spleen, lung, and kidney) were taken and stained with hematoxylin−eosin (H&E) to perform the histological assay. The results were observed under an Olympus CX43 microscope (Japan). All animals were handled in strict accordance with the Guide for the Care and Use of Laboratory Animals, and the procedures were approved by the University Committee on the Use of Animals of Guangdong University of Technology of China.

Supplementary Figures

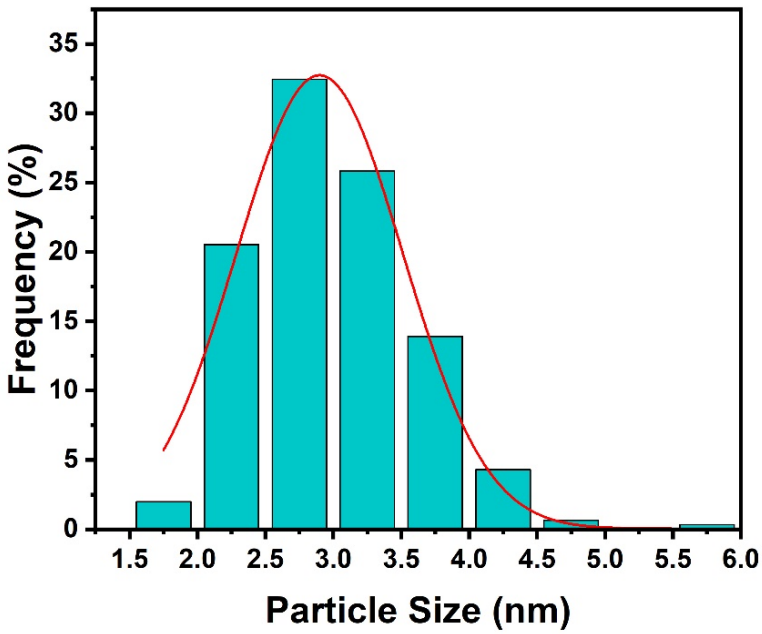

Figure S1. Particle size distribution of Rh@CPA NPs based on 302 particles, and the average diameter of ca. 2.9 nm.

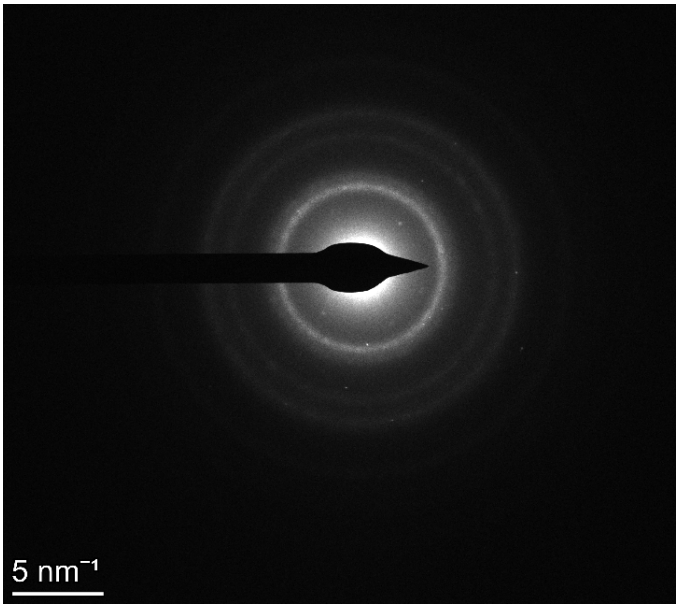

Figure S2. The selected area electron diffraction pattern (SAED) of Rh@CPA NPs.

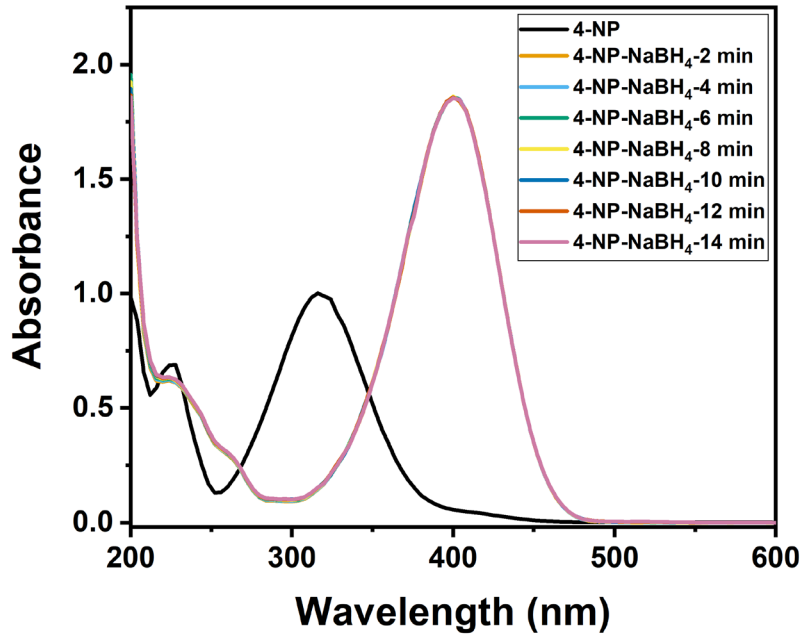

Figure S3. UV-vis spectra of freshly prepared 4-nitrophenol (4-NP) and after addition of $NaBH_4$.

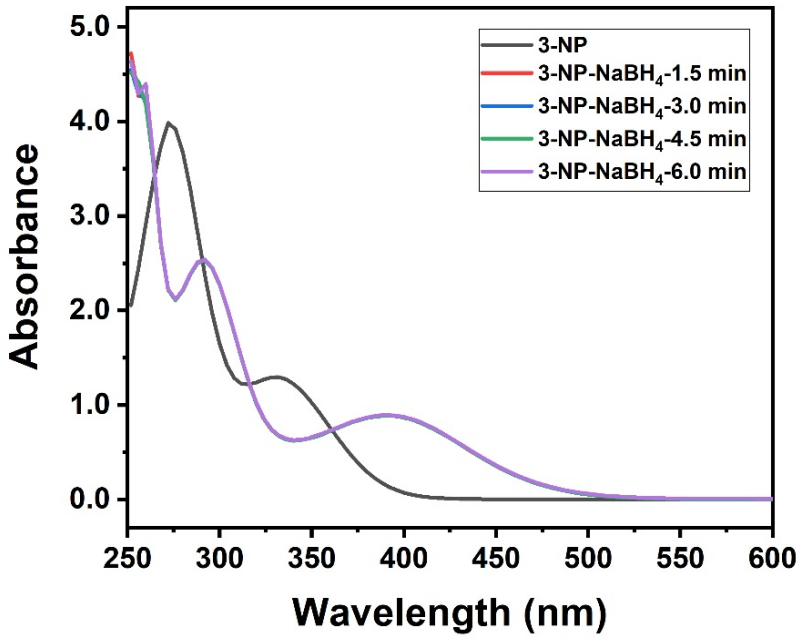

Figure S4. UV-vis spectra of freshly prepared 3-nitrophenol (3-NP) and after addition of $NaBH_4$.

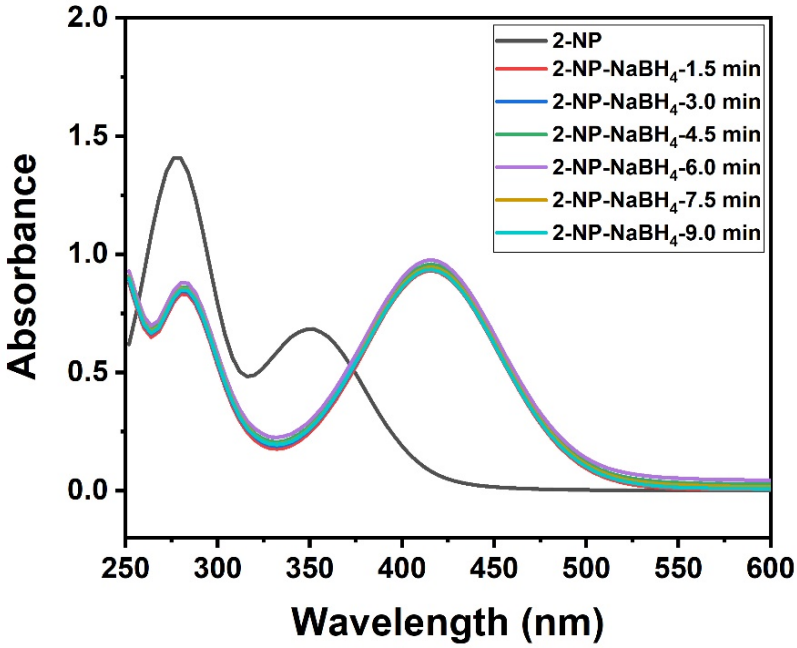

Figure S5. UV-vis spectra of freshly prepared 2-nitrophenol (2-NP) and after addition of $NaBH_4$.

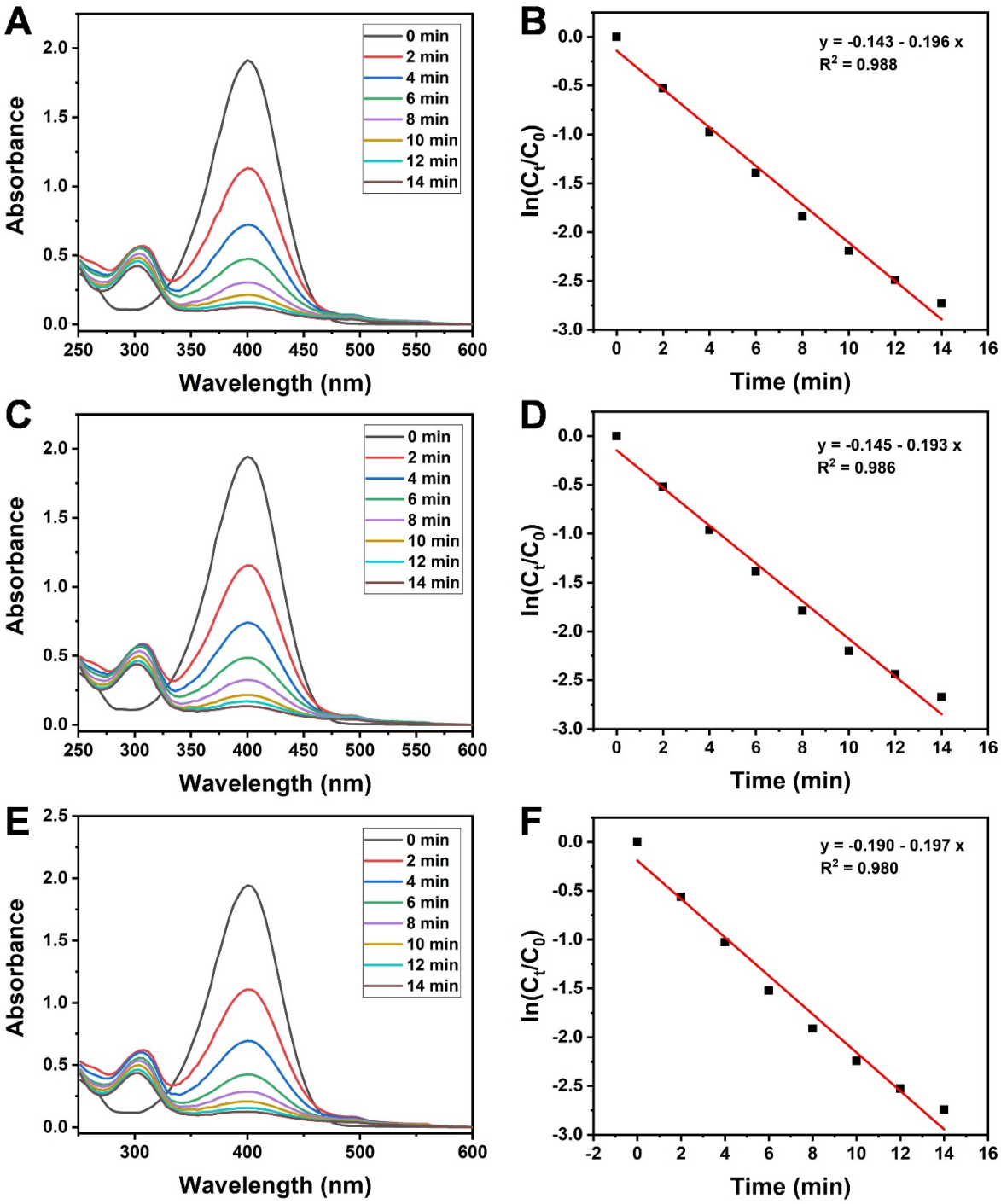

Figure S6. Time-dependent UV-vis absorption spectra of 4-nitrophenol solution reduced by $NaBH_4$ using Rh@CPA as a catalyst and the corresponding $\ln(C_t/C_0)$ versus time for the catalytic reduction.

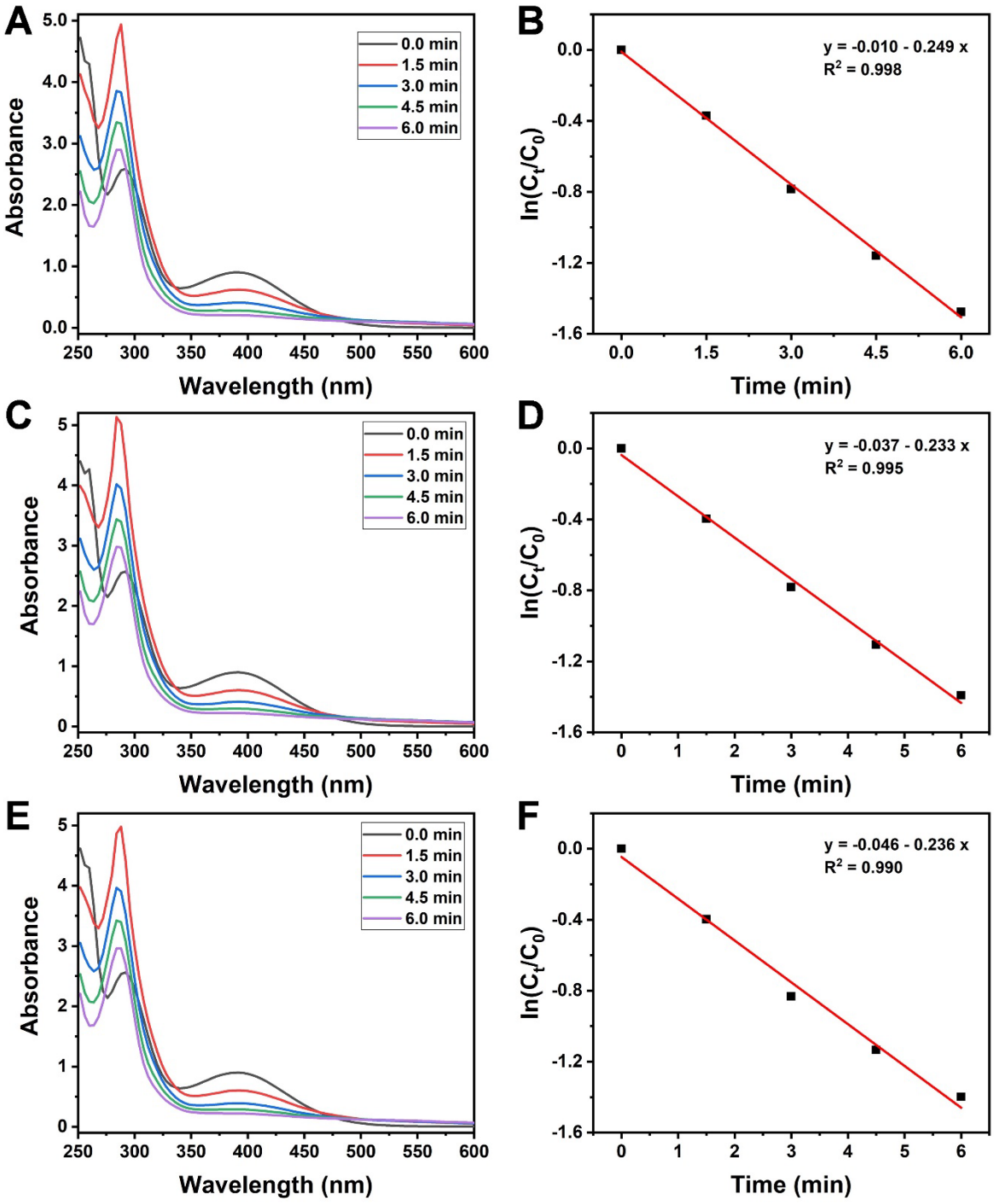

Figure S7. Time-dependent UV-vis absorption spectra of 3-nitrophenol solution reduced by $NaBH_4$ using Rh@CPA as a catalyst and the corresponding $\ln(C_t/C_0)$ versus time for the catalytic reduction.

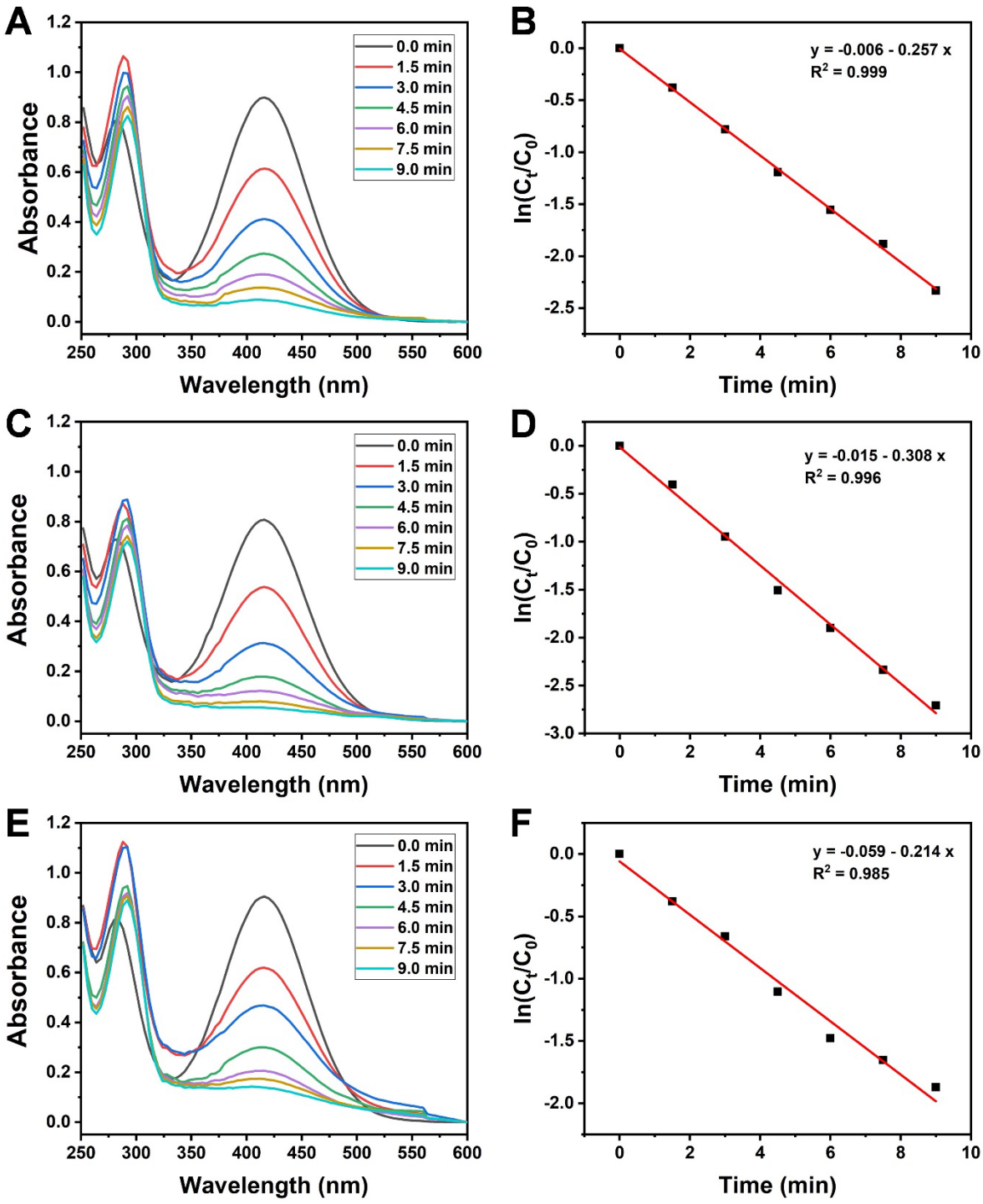

Figure S8. Time-dependent UV-vis absorption spectra of 2-nitrophenol solution reduced by $NaBH_4$ using Rh@CPA as a catalyst and the corresponding $\ln(C_t/C_0)$ versus time for the catalytic reduction.

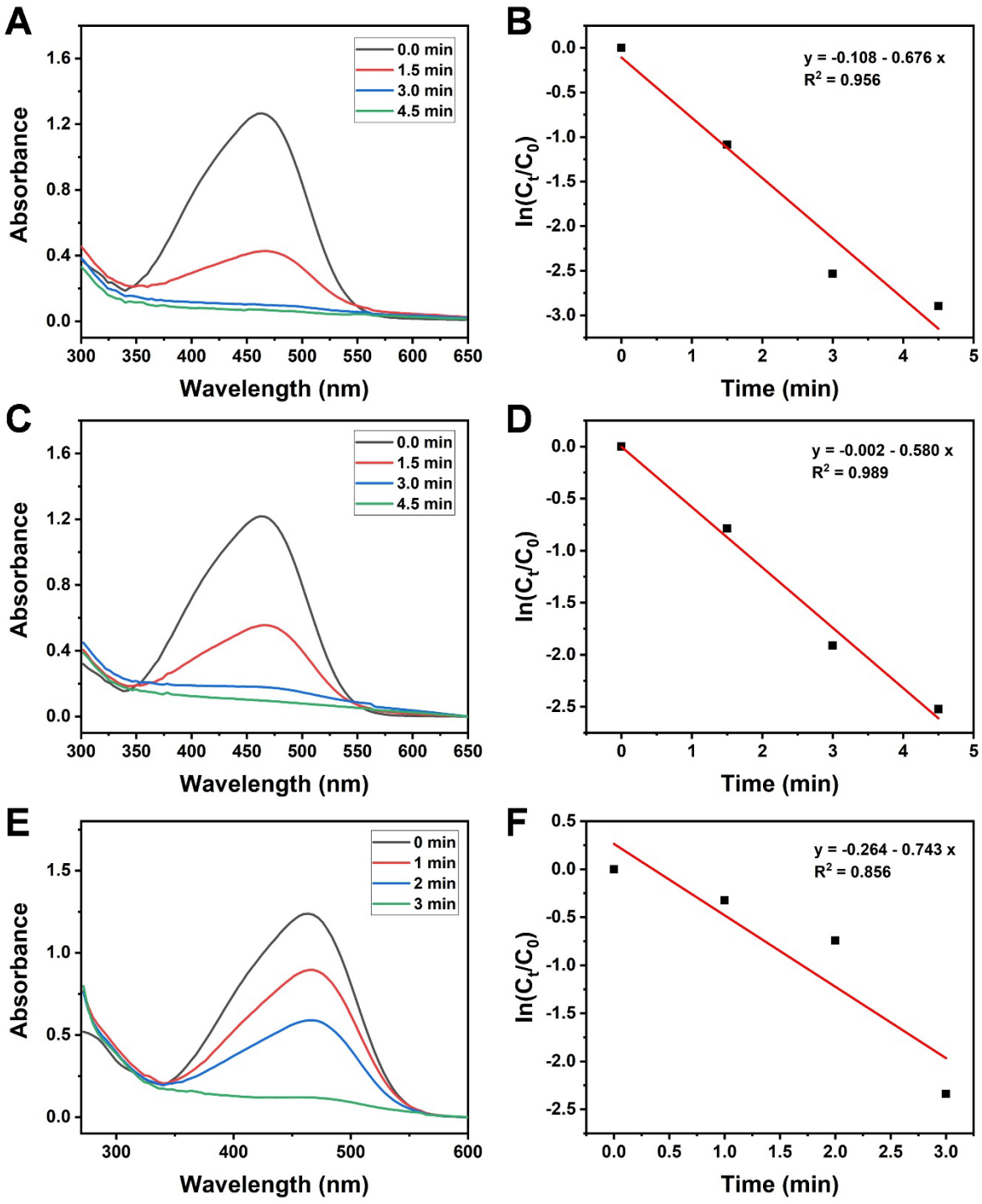

Figure S9. Time-dependent UV-vis absorption spectra of MO solution reduced by $NaBH_4$ using Rh@CPA as a catalyst and the corresponding $\ln(C_t/C_0)$ versus time for the catalytic reduction.

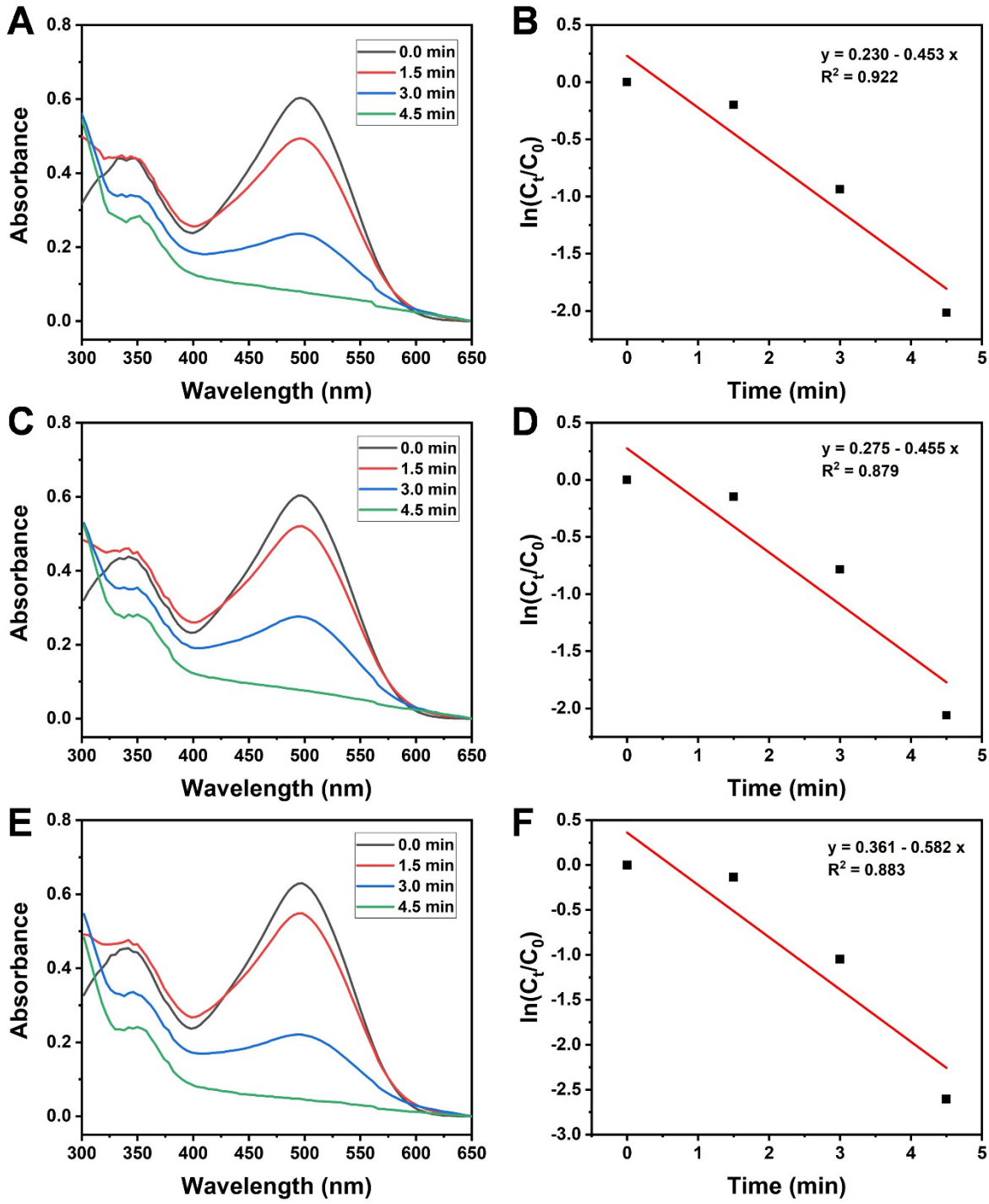

Figure S10. Time-dependent UV-vis absorption spectra of CR solution reduced by $NaBH_4$ using Rh@CPA as a catalyst and the corresponding $\ln(C_t/C_0)$ versus time for the catalytic reduction.

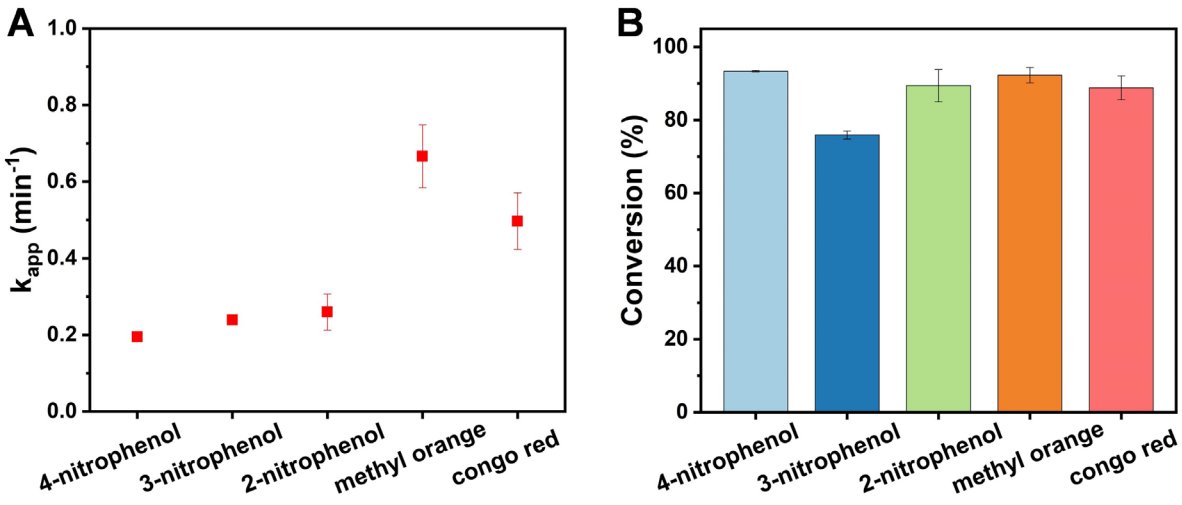

Figure S11. (A) Rate constants for the catalytic reductions of nitrophenols and azo dyes using Rh@CPA as a catalyst and its error analysis; (B) Conversion efficiency for the catalytic reductions of nitrophenols and azo dyes using Rh@CPA as a catalyst and its error analysis.

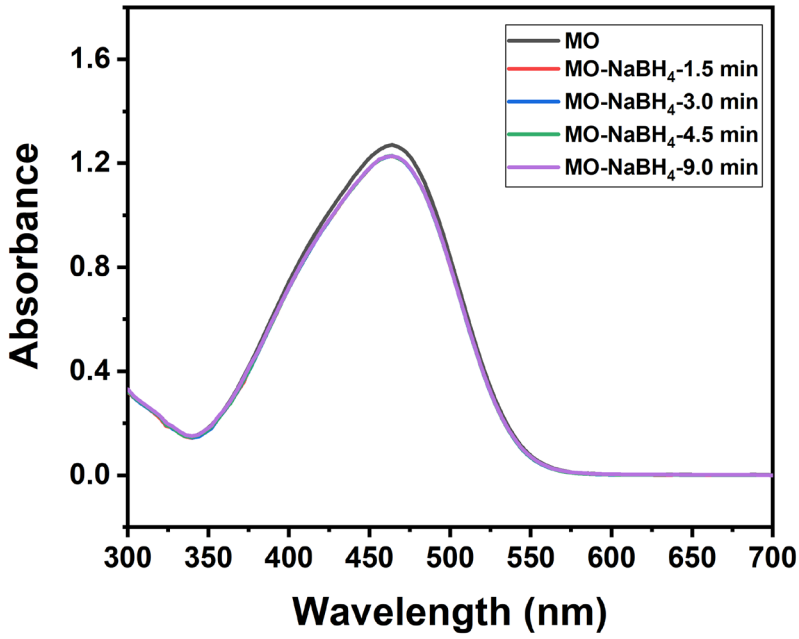

Figure S12. UV-vis spectra of freshly prepared MO and after addition of $NaBH_4$.

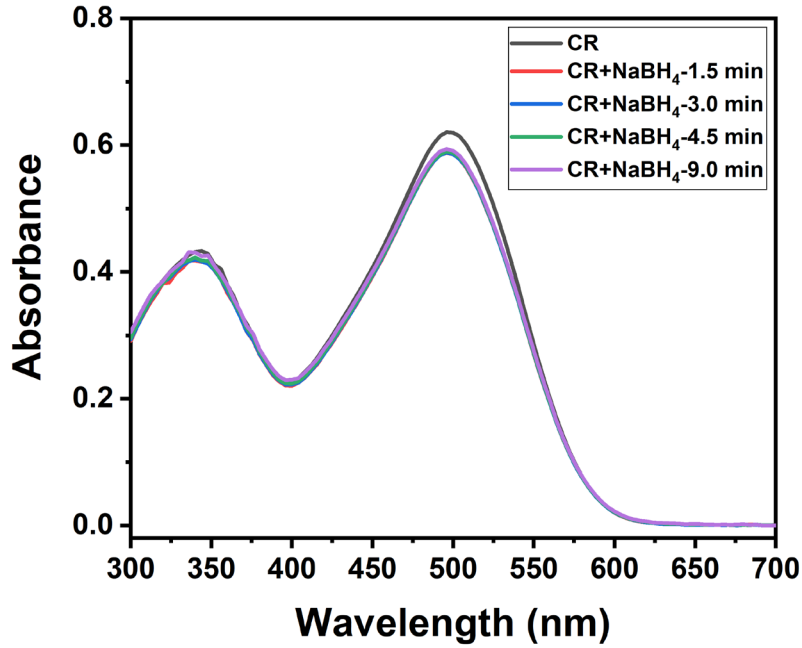

Figure S13. UV-vis spectra of freshly prepared CR and after addition of $NaBH_4$.

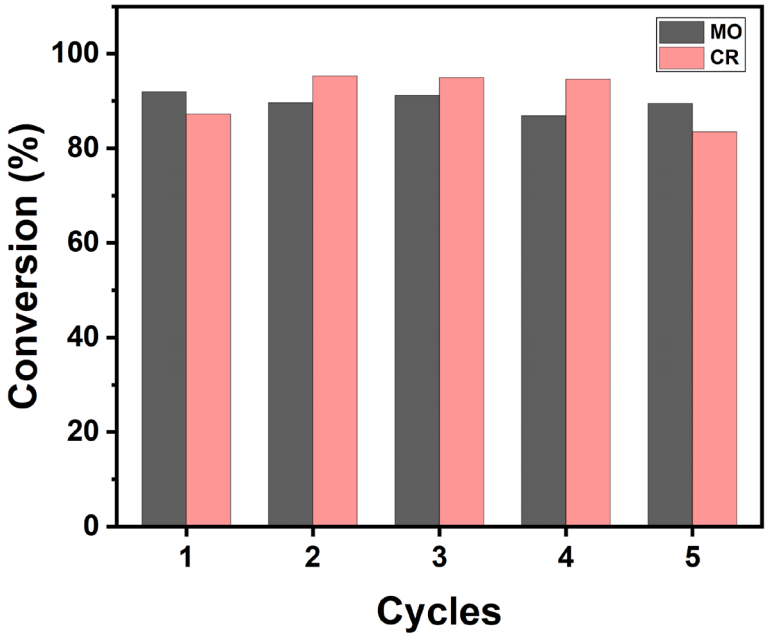

Figure S14. Recyclable catalytic performance of Rh@CPA for the reduction of MO and CR over 5 cycles.

Table S2. Comparison of catalytic rates for the reduction of nitro compounds using different metal NPs as catalysts.

Metal NPs	Capping agent/support	Nitro compounds	Rate constant values (min^{-1})	Ref. number in present paper
Rh	CTAB	4- nitroaniline	0.34×10^{-1}	S4
Rh	Deoxyribonucleic acid (DNA)	4- nitroaniline	2.17×10^{-1}	S5
Rh	Dendrimer	4-nitrophenol	3.84×10^{-1}	S6
Rh	Dendritic mesoporous silica nanospheres	4-nitrophenol	2.60×10^{-1}	S7
Rh	Carbon nanosheets	4-nitrophenol	1.86×10^{-1}	S8
Rh	Fullerene-C60	4-nitrophenol	1.32×10^{-1}	S9
Rh	Graphene quantum dots	4-nitrophenol	1.68×10^{-1}	S10
Rh	Carboxylated pillar[5]arene	4-nitrophenol	1.95×10^{-1}	This work
Rh		3-nitrophenol	2.39×10^{-1}	This work
Rh		2-nitrophenol	2.60×10^{-1}	This work
Au	Carboxylated pillar[6]arene	4-nitrophenol	1.19×10^{-1}	S11
Au	Cucurbit[7]uril	4-nitrophenol	0.84×10^{-1}	S12
Ag	Carboxylated leaning tower[6]arene	4-nitrophenol	2.83×10^{-1}	S13
Ag	2-hydroxypropyl-β-cyclodextrin	4-nitrophenol	0.91×10^{-1}	S14
Ag	Leaf extract of Terminalia arjuna	4-nitrophenol	1.42×10^{-1}	S15

Pt	β-cyclodextrin	4-nitrophenol	8.8×10^{-1}	S16
Pt	Ascorbic acid	4-nitrophenol	1.25×10^{-5}	S17
Pd	Alkyne-terminated calixarene	4-nitrophenol	1.19×10^{-1}	S18
Pd	Bis-azide calixarene	4-nitrophenol	4.63×10^{-1}	S18
Pd	Glucosamine	4-nitrophenol	0.80×10^{-1}	S19
RuCu	β-cyclodextrin	4-nitrophenol	2.10×10^{-1}	S20

Table S3. Comparison of catalytic rates for the reduction of MO using different metal NPs as catalysts.

Metal NPs	Capping agent/support	Rate constant values (min^{-1})	Ref. number in present paper
Rh	Carboxylated pillar[5]arene	6.66×10^{-1}	This work
Au	L-asparagine	3.14×10^{-1}	S21
Au	Tannic acid	0.49×10^{-2}	S22
Ag	Tannic acid	5.85×10^{-1}	S22
Ag	CTAB	2.10×10^{-1}	S23
Ag	Leaf extract of Terminalia arjuna	1.66×10^{-1}	S15
Pt	Tannic acid	0.29×10^{-2}	S22
Fe	EDTA	0.77×10^{-1}	S24
Fe_3Pt-Ag	Polyethyleneimine dithiocarbamate	2.30×10^{-1}	S25

Table S4. Comparison of catalytic rates for the reduction of CR using different metal NPs as catalysts.

Metal NPs	Capping agent/support	Rate constant values (min^{-1})	Ref. number in present paper
Rh	Carboxylated pillar[5]arene	4.97×10^{-1}	This work
Au	Leaf extract of Synedrella nodiflora	1.63×10^{-1}	S26
Ag	Leaf extract of Synedrella nodiflora	1.84×10^{-1}	S26
Co	The Melia Azedarach (MA) plant materials	0.61×10^{-1}	S27
Ni	Mesoporous N-doped carbon	7.14×10^{-1}	S28

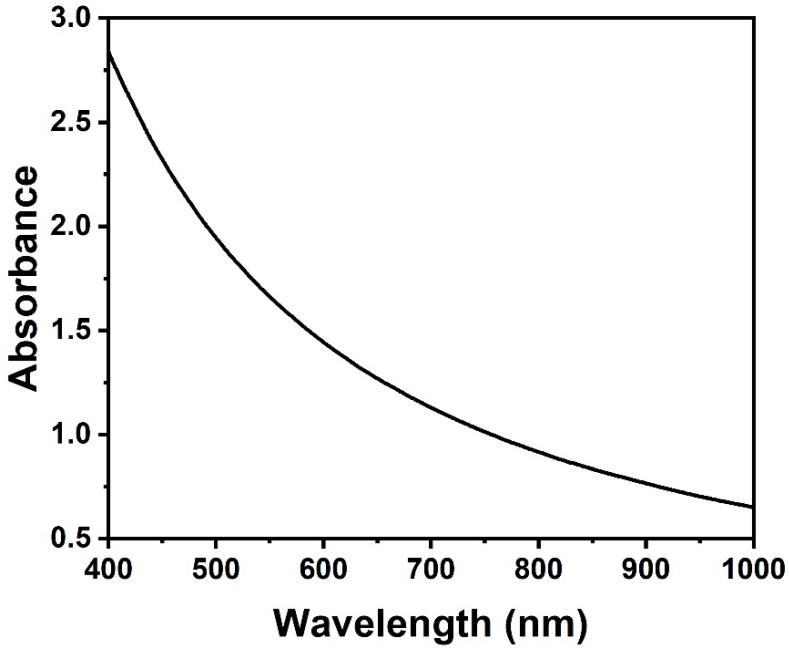

Figure S15. UV-vis-NIR spectrum of Rh@CPA solution (29.6 μg/mL) in a quartz cuvette with a path length of 1 cm.

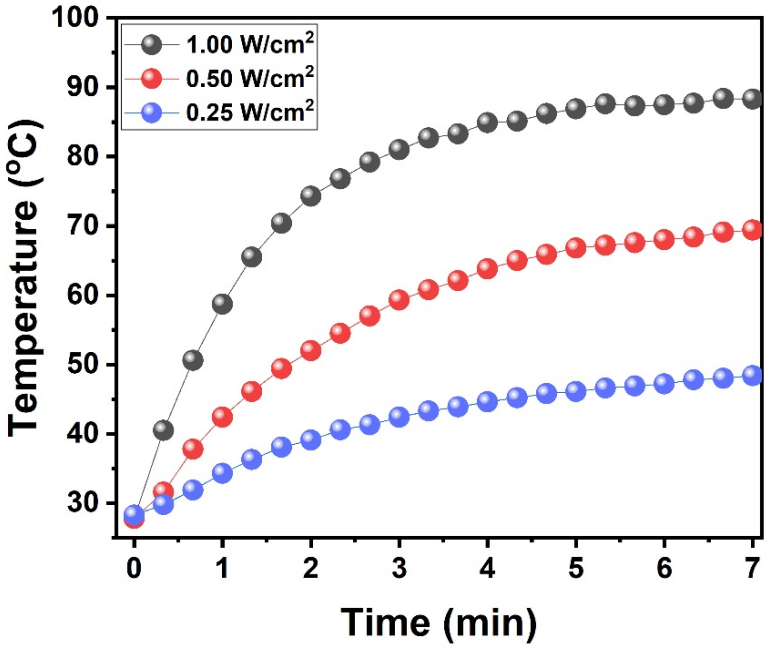

Figure S16. Temperature change curves of Rh@CPA NPs solutions (29.60 μg/mL) upon irradiation of 808 nm laser with different power density.

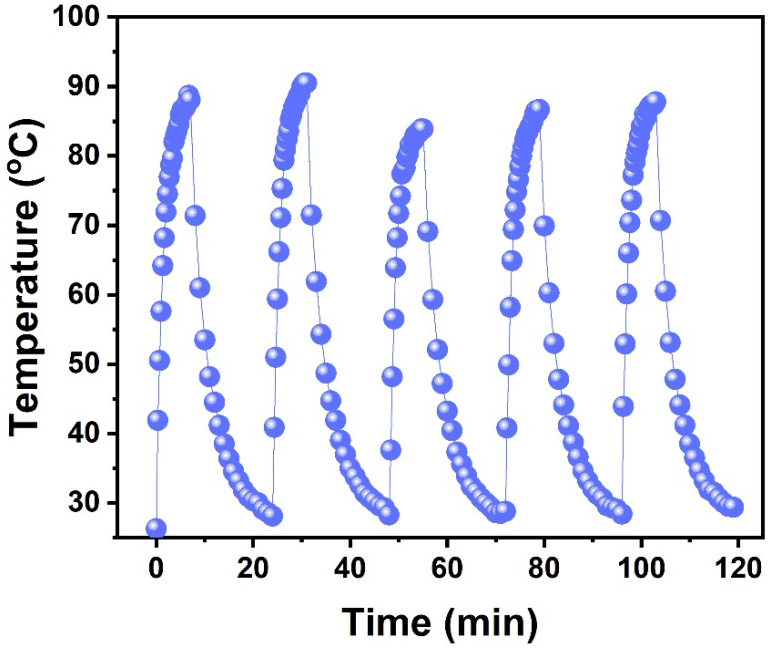

Figure S17. The temperature evolution cycles of Rh@CPA solution (29.6 μg/mL) under periodic NIR laser ON/OFF irradiation (1.0 W/cm^2).

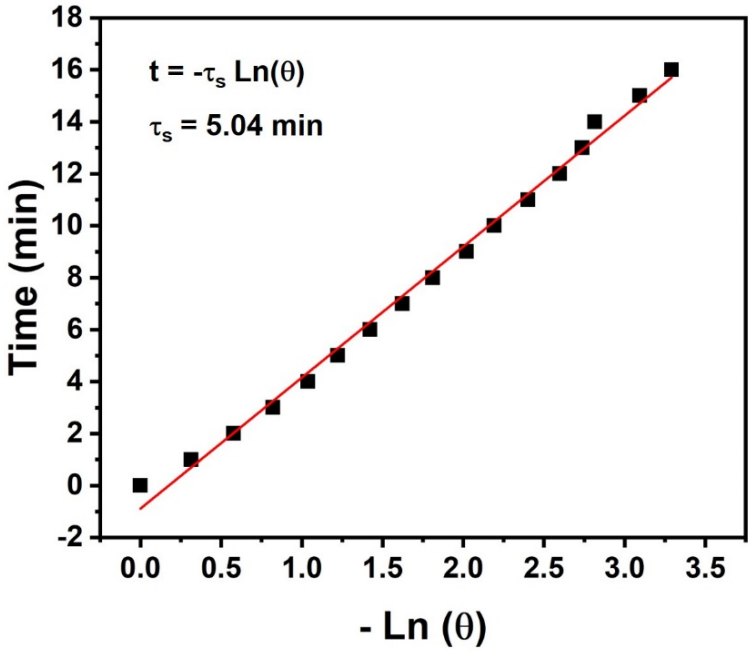

Figure S18. The plot of cooling time versus negative natural logarithm of driving force temperature.

References

S1. H. Li, D.-X. Chen, Y.-L. Sun, Y. B. Zheng, L.-L. Tan, P. S. Weiss and Y.-W. Yang, *J. Am. Chem. Soc.*, 2013, **135**, 1570–1576.

S2. D. K. Roper, W. Ahn and M. Hoepfner, *J. Phys. Chem. C*, 2007, **111**, 3636−3641.

S3. Q.-L. Li, Y. Sun, L. Ren, X. Wang, C. Wang, L. Li, Y.-W. Yang, X. Yu and J. Yu, *ACS Appl. Mater. Interfaces*, 2018, **10**, 29314–29324.

S4. S. Kundu, K. Wang and H. Liang, *J. Phys. Chem. C*, 2009, **113**, 18570–18577.

S5. S. Kundu, Y. Chen, W. Dai, L. Ma, A. M. Sinyukov and H. Liang, *J. Mater. Chem. C*, 2017, **5**, 2577–2590.

S6. X. Liu, J. Ruiz and D. Astruc, *J. Inorg. Organomet. Polym.*, 2018, **28**, 399–406.

S7. J. Tian, D. Yang, J. Wen, A. S. Filatov, Y. Liu, A. Lei and X.-M. Lin, *Nanoscale*, 2018, **10**, 1047–1055.

S8. C. Lin, G. Wu, H. Li, Y. Geng, G. Xie, J. Yang, B. Liu and J. Jin, *Nanoscale*, 2017, **9**, 1834–1839.

S9. M. Gopiraman, S. Saravanamoorthy, S. Ullah, A. Ilangovan, I. S. Kim and I. M. Chung,

RSC Adv., 2020, **10**, 2545–2559.

S10. N. Li, W. Chen, J. Shen, S. Chen and X. Liu, *Inorg. Chim. Acta*, 2019, **496**, 119031.

S11. X. Wang, Z.-J. Liu, E. H. Hill, Y. Zheng, G. Guo, Y. Wang, P. S. Weiss, J. Yu and Y.-W. Yang, *Matter*, 2019, **1**, 848–861.

S12. E. Blanco, I. Esteve-Adell, P. Atienzar, J. A. Casas, P. Hernández and C. Quintana, *RSC Adv*., 2016, **6**, 86309–86315.

S13. Y. Zhang, Z. Li, S. Meng, A. Dong and Y.-W. Yang, *Chem. Commun*., 2022, **58**, 649–652.

S14. T.-D. Nguyen, C.-H. Dang and D.-T. Mai, *Carbohyd. Polym*., 2018, **197**, 29–37.

S15. S. Raj, H. Singh, R. Trivedi and V. Soni, *Sci. Rep*., 2020, **10**, 9616.

S16. L. Xian, B.-Q. Su, Y.-X. Feng, B. Xi and Z.-Y. Duan, *Inorg. Nano-Met. Chem*., 2021, **51**, 882–888.

S17. J. Wang, X.-B. Zhang, Z.-L. Wang, L.-M. Wang, W. Xing and X. Liu, *Nanoscale*, 2012, **4**, 1549-1552.

S18. V. Burilov, D. Mironova, E. Sultanova, R. Garipova, V. Evtugyn, S. Solovieva and I. Antipin, *Molecules*, 2021, **26**, 6864.

S19. S. Ullah, A. Ahmad, A. Khan, J. Zhang, M. Raza, A. ur Rahman, M. Tariq, U. A. khan, S. Zada and Q. Yuan, *Microb. Pathogenesis*, 2018, **125**, 150–157.

S20. L. Bai, *Dalton Trans*., 2016, **45**, 4712–4715.

S21. N. Garg, S. Bera, L. Rastogi, A. Ballal and M.V. Balaramakrishna, *Spectrochim. Acta A*, 2020, **232**, 118126

S22. N. Gupta, H. P. Singh and R. K. Sharma, *J. Mol. Catal. A- Chem*., 2011, **335**, 248–252.

S23. Z. Zaheer and E. S. Aazam, *J. Mol. Liq*., 2017, **242**, 1035–1041.

S24. K. V. G. Ravikumar, S. Dubey, M. pulimi, N. Chandrasekaran and A. Mukherjee, *J. Mol. Liq*., 2016, **224**, 589–598.

S25. D. Han, B. Li, G. Xing, Y. Zhang, Y. Chen, Y. Sun, Y. Zhang, Y. Liu and J. Yang, *Chem. Res. Chin. Univ*., 2018, **34**, 871–876.

S26. R. Vijayan, S. Joseph and B. Mathew, *IET Nanobiotechnol.*, 2018, **12**, 850–856.

S27.Z. Ahmad, S. A. Shah, I. Khattak, H. Ullah, A. A. Khan, R. A. Shah, S. A. Khan and S. B. Khan, *J. Mater. Sci- Mater. El*., 2020, **31**, 16938–16950.

S28. Z. Lv, W. Chen, Y. Cai, K. Chen, K. Li, M. Fang, X. Tan and X. Wang, *Appl. Surf. Sci*., 2022, **575**, 151748.